Assignment

Homelab HL2

Alberto Doimo 10865196
Riccardo Iaccarino 10868500

Musical Acoustics

POLITECNICO
MILANO 1863

December 4, 2023

a) Design of the resonator

The Helmoltz resonator in Fig.1 is described by the following dimensions:

- Main chamber diameter D
- Neck length $l_1 = 1$ $[cm]$
- Neck diameter $d_1 = 4$ $[cm]$

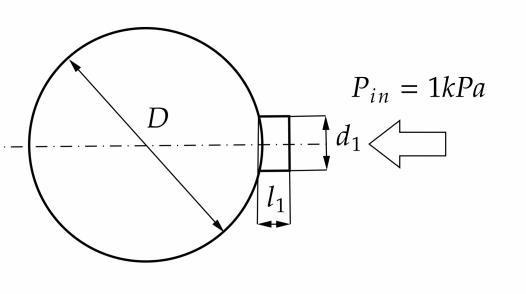

Figure 1: Helmoltz resonator scheme

Firstly it is required to obtain analytically the diameter D that corresponds to a resonance frequency $f_1 = 300$ $[Hz]$.

To do so the equation for the natural frequency of vibration of an Helmholtz resonator was used:

$$f_1 = \frac{c}{2\pi}\sqrt{\frac{S}{VL}} \tag{1}$$

in which we can recognize respectively the cross-section S and the length L of the neck and the volume V of the air cavity. A crucial observation has to be done on L: since the neck can be seen as a pipe, we have to introduce a correction to the length of the ideal case in order to include radiation losses. In particular we chose to add a virtual elongation of $\Delta L = 0.93 \cdot d_1/2$, which will be deeper discussed in the following section. Substituting for D, which is present in the expression of V and taking into account that $S = \pi(d_1/2)^2$, we can obtain the diameter of the chamber as:

$$D = \frac{1}{\pi}\sqrt[3]{\frac{3Sc^2}{2Lf_1{}^2}} \tag{2}$$

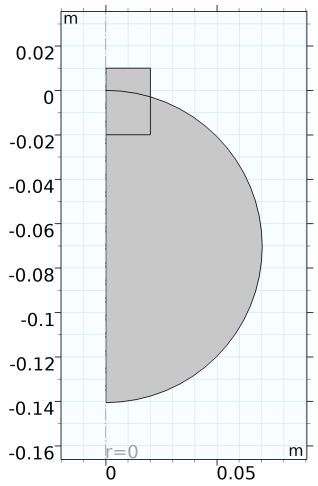

Figure 2: 2D geometry definition

Once D was obtained, the COMSOL model was created in order to simulate the Helmholtz resonator's behaviour. The geometry was defined as a 2D axial symmetric component, since the 3D model was then automatically created by rotating the 2D figure around the z-axis. The resonator is defined as in Fig.2 by the union of an half circle and a rectangle that extends along the z-axis over $D/2$ positively by l_1 and negatively by two times l_1 to always intersect the circle, even when d_1 varies in point c). In order to correctly carry on the simulation some features were necessarily added; the *material* is defined as air, then the *Pressure acoustics, frequency domain* physics

was added and the *viscous* fluid model was selected. An input pressure $P_{in} = 1$ $[KPa]$ is applied as shown in Fig.1 to the resonator.

b) Frequency sweep analysis

The mesh was defined by applying first of all the *edge* mesh property at all the edges of the 2D geometry, except for the upper one, where the pressure P_1 is applied. A *free triangular* mesh is then created over the surface: in order to properly simulate the behaviour of the resonator, the *size* of the mesh must be under the smallest wavelength considered in the performed sweep. Since the maximum frequency of interest is $10[kHz]$, the mesh size must respect the following condition:

$$l_{el,max} < \frac{\lambda}{8} = \frac{343}{8 \cdot 10000} = 0.0043[m] \tag{3}$$

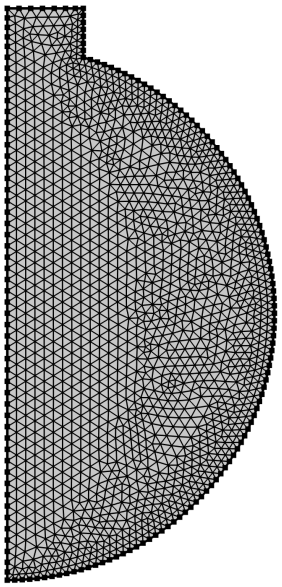

Figure 3: Mesh of the resonator

This condition was satisfied by selecting a sufficiently fine mesh, with a maximum element size of $l_{el,max} = 0.003$ $[m]$. The resulting mesh is shown in Fig.3. At this point the frequency sweep analysis can be computed by creating a *frequency domain* study from $10[Hz]$ to $10[kHz]$ with $10[Hz]$ steps. In order to visualize the results of the simulations, some *probes* were defined: *total acoustic pressure* = P $[Pa]$; *total acoustic velocity* = U_z $[m^3/s]$ (along the z-axis); both probes were applied to the resonator entrance (upper edge) to obtain the input impedance as:

$$Z = \frac{P}{U_z} \; [Ns/m^5] \tag{4}$$

(Notice that in all the plots the impedance magnitude $|Z|$ will be represented in a dB scale). The result, described by Fig.4, shows that there is a minimum of the impedance at $300[Hz]$ which corresponds to the resonance frequency of the system. This results has been obtained by tuning the coefficient of the virtual elongation ΔL to a value of 0.93, in order compensate for the radiation losses of the ideal pipe w.r.t. the real case. The graphs on the left show the magnitude and phase responses of the input impedance obtained from the COMSOL simulation, on the right there is a zoom on the resonance zone. The frequency response from the first resonance up to the $10[kHz]$ simulation limit shows an interesting behaviour: there is a succession of peaks that repeat in an harmonic pattern; this is given by the neck and sphere harmonics that progressively overlap towards the upper frequency limit to the point in which they are completely mixed together.

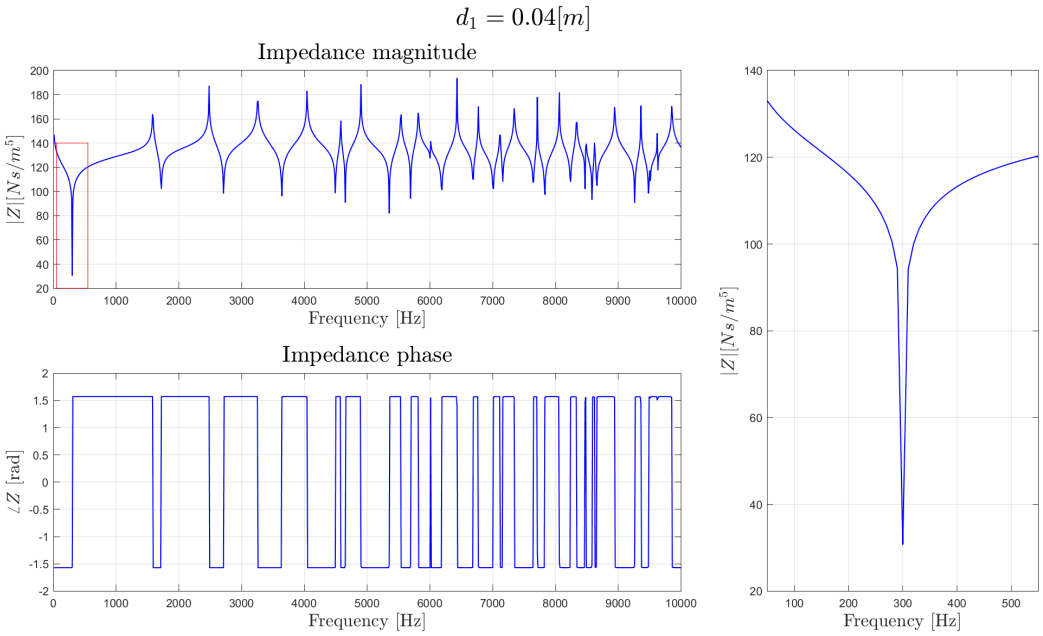

Figure 4: Impedance plot of the system with zoom on its first resonance

c) Analysis of the modified resonator's neck diameter

The following study was carried out in order to analyze how the neck diameter influences the frequency response. To perform this analysis we computed a *parametric sweep* over $d_1 = [1, 3, 8]\ [cm]$, keeping every other parameter constant and the same *probes* already defined in *b)*. The results are ordered in Fig.5 with increasing diameter from top to bottom. The column on the right highlights in correspondence of which frequencies f_1 and f_2 the first two resonances can be found.

	$d = 1[cm]$	$d = 3[cm]$	$d = 8[cm]$
f_1	$110[Hz]$	$250[Hz]$	$470[Hz]$
f_2	$1640[Hz]$	$1690[Hz]$	$1850[Hz]$

Table 1: First two resonance frequency for $d_1 = [1, 3, 8]\ [cm]$

We can notice how the values in Tab.1 (specifically the first row) are related to the neck's cross-section S by relation (1). In particular, the resonance frequency grows with the diameter d_1, since it is directly proportional to $\sqrt{S}$, where $S = \pi(d_1/2)^2$. It is however interesting to see how the frequency increase rate is not linear w.r.t. the diameter (e.g. when d_1 triples, the frequency becomes not much more than twice the previous one). This happens due to the fact that f_1 is also inversely proportional to L, which is in its turn related to the diameter d by the virtual elongation ΔL already described at point b).

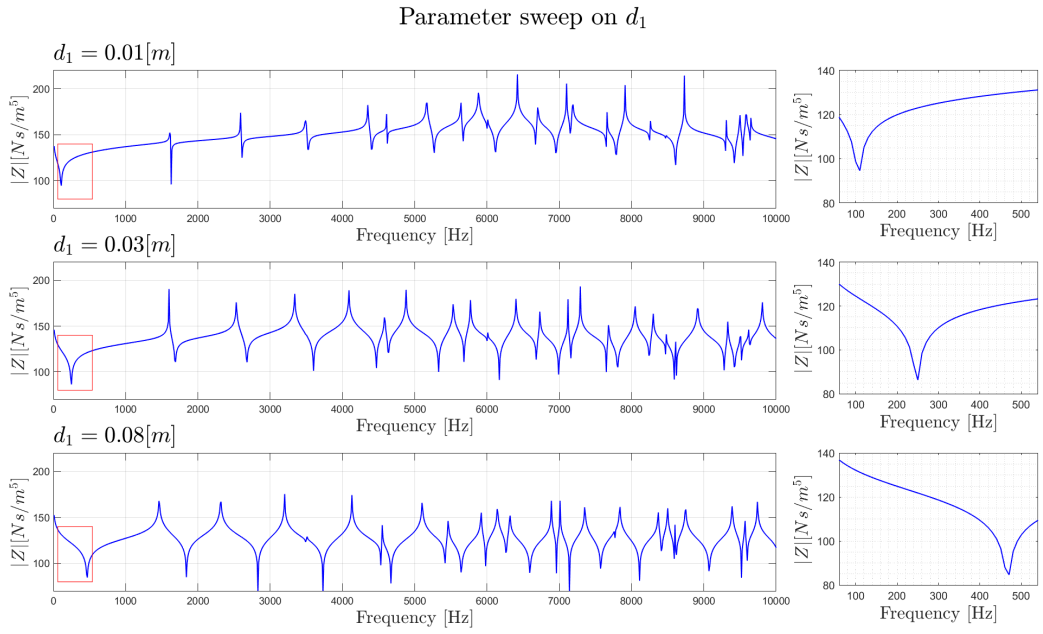

Figure 5: Impedance magnitude trends for different values of d_1, first resonance on the right

Some results obtained from the COMSOL simulation can be seen in Fig.6: here the total acoustic pressure is displayed in the resonator's section. The exact values of the first two resonance frequencies for the four analyzed diameters are reported in Tab.1. We can notice how for each diameter the same pressure areas can be identified: at the first resonance (left) we can observe an in-phase movement of all the volume, instead for the second one the pressure field is composed of two parts with opposite phase separated by a nodal line. By looking at the COMSOL simulation this can be interpreted as the first nodal line going progressively down from the top into the cavity as the frequency goes up; we will discuss this behaviour also in the second part of the report.

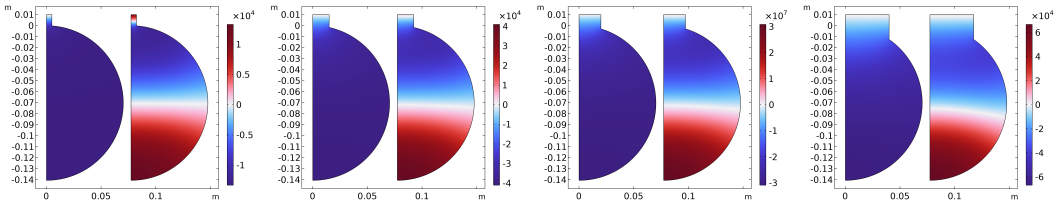

Figure 6: Distribution of acoustic pressure in the resonator at the first two resonances for $d_1 = [1, 3, 4, 8]$ $[cm]$

d) Modal analysis

In this section we performed a modal analysis by varying the *azimuthal mode number* parameter of the *Pressure acoustics, frequency domain* physics. The considered values are $m = [0, 1, 2, 3]$ and the results for all the modes are shown in Fig.7 for $d_1 = 1$ $[cm]$, Fig.8 for $d_1 = 3$ $[cm]$, Fig.9 for $d_1 = 8$ $[cm]$. The first comment that can be made is about the

type of excitation of the different well-known azimuthal modes of a pipe: the mode 0 always allows the different resonances to be excited by P_{in} applied to the resonantor's entrance and so the impedance graph is populated up to $10[kHz]$; in the case of the mode 1,2,3 instead the graph doesn't show any resonance for the smallest diameter $d_1 = 1$ $[cm]$ and progressively populates as the diameter size increases. This general trend is recognizable for all the studied cases and suggests a relationship between frequency, mode number and diameter size. Interestingly a similar behaviour can be encountered for an ideal infinite pipe, where the cutoff frequency ω_c is inversely proportional to the pipe radius, while it increases as the mode number. We can therefore deduce that also in this case the relation holds, since the volume of the chamber is kept constant and the only changing parameters are associated to the neck dimensions. This justifies why for every considered diameter some plots have no peaks (for example in Fig.8 the third mode) or there are peaks only above a certain frequency that can be assumed to be the cutoff one, as visible for example in Fig.8 for the second mode.

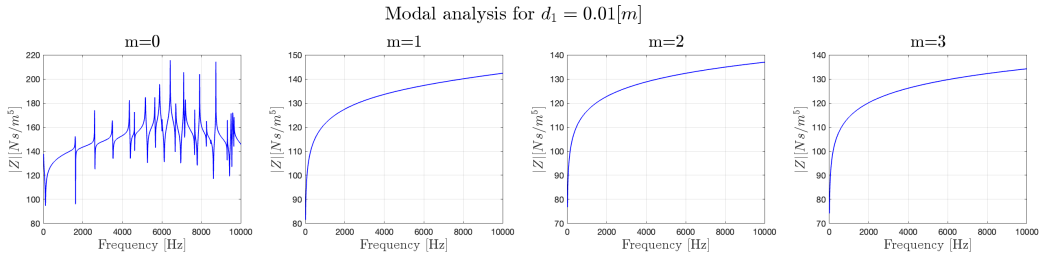

Figure 7: Impedance magnitude of the first four modes for $d_1 = 0.01$ $[m]$

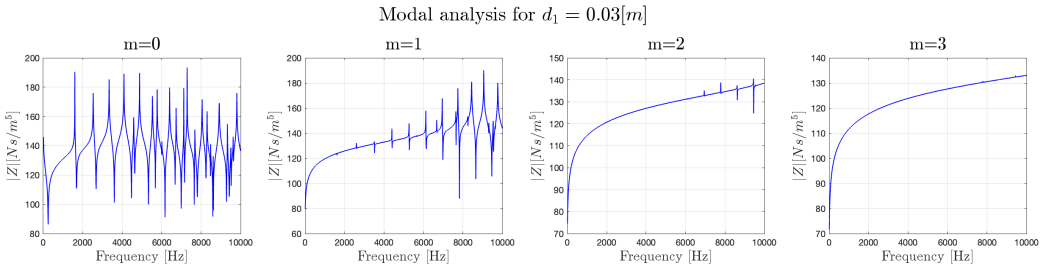

Figure 8: Impedance magnitude of the first four modes for $d_1 = 0.03$ $[m]$

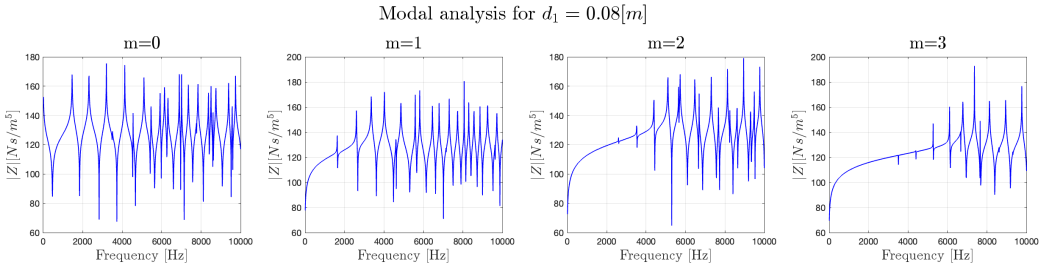

Figure 9: Impedance magnitude of the first four modes for $d_1 = 0.08$ $[m]$

Some considerations can now be made about what geometry is the best one for an Helmholtz resonator. In order to do this it is better to look at the sum of all the considered modes in the studied frequency range, because even if the diameter $d_1 = 1$ $[cm]$ appears to be the less noisy one in terms of resonances, the sum all the modes for the other diameter components could result in a better final configuration. These comparison can be seen in Fig.10, Fig.11, Fig.12, respectively for $d_1 = [1, 3, 8]$ $[cm]$. We can confirm that the first configuration must be preferred among the three, since the sum doesn't provide any cancellation in terms of resonances and so no improvements, but it instead creates an even richer harmonic profile. The presence of many resonant peaks must be avoided, in order to have a resonator that absorbs signals only at the resonance frequency and possibly has no effect anywhere else. It is then clear how in Fig.11 and Fig.12 there are many more peaks than in Fig.10, and so these two configuration must be discarded.

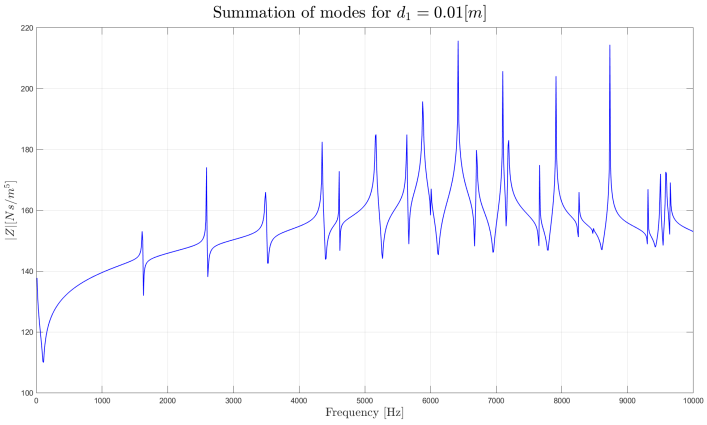

Figure 10: Summation of modes of the impedance magnitude for $d_1 = 0.01$ $[m]$

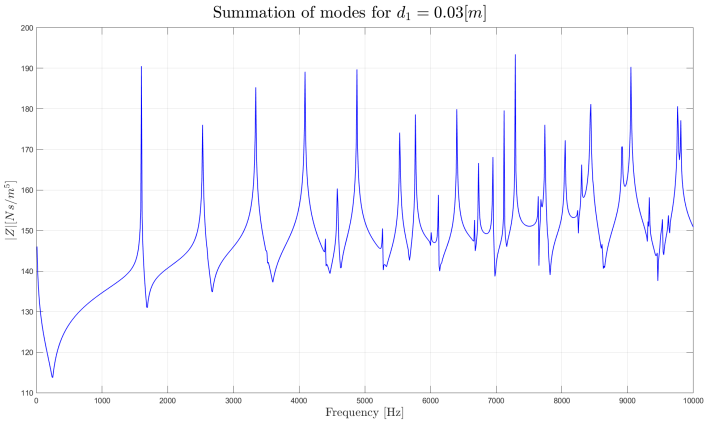

Figure 11: Summation of modes of the impedance magnitude for $d_1 = 0.03$ $[m]$

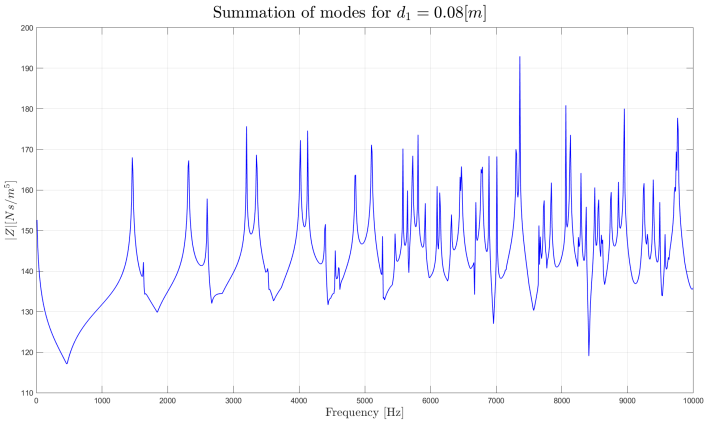

Figure 12: Summation of modes of the impedance magnitude for $d_1 = 0.08$ $[m]$

e) Double resonator configuration

From now on, we will deal with a new system which includes the introduction of a second Helmholtz resonator, attached to the previous one's closed end with its neck, as can be seen in Fig.13. The dimensions of the original resonator will be those of the one we selected in the previous point (i.e. $d_1 = 0.01$ $[m]$); whereas the second one is described by:

- Air cavity diameter $D_2 = 15.86$ $[cm]$
- Neck length $l_2 = 2l_1 = 2$ $[cm]$
- Neck diameter $d_2 = 4$ $[cm]$

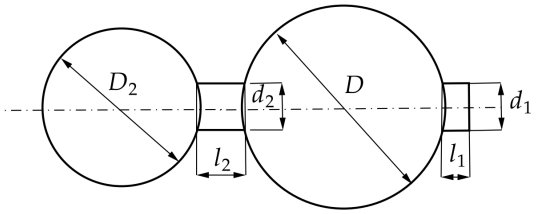

Figure 13: Scheme for the double configuration

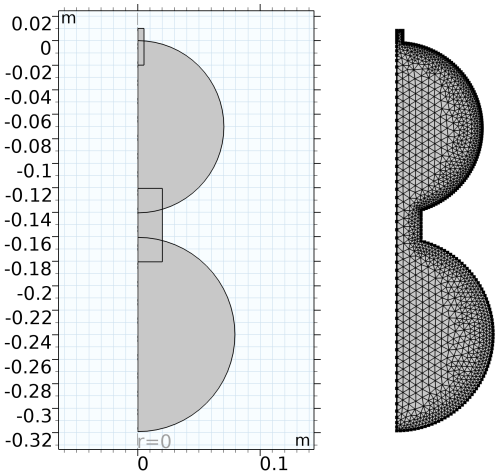

Figure 14: Geometry and mesh of the new composite system

The implementation of this geometry in COMSOL has been done in a similar way w.r.t. the single element already studied. In particular, in order to ensure that the neck in the middle would not cause any problem related to an incorrect connection, we extended its length of three times before merging the components. The next step is creating a proper mesh, for which we can take as reference the process discussed in section b, extending the *edge* selection to the boundaries of the second resonator. From the final output shown in Fig.14 it is evident how the mesh results finer along the edges of the system than how it is towards the center; another peculiarity is given instead by the higher element density that characterizes the upper resonator, due to its smaller neck and cavity.

At this point we can apply the very same physics conditions of the previous studies and we can define the probes that will gather for us the information about acoustic pressure and acoustic velocity on the external interface. The study performed is once again a *parametric sweep* on the first four modes, but the results reported in Fig.15 directly show their sum: we preferred to exclude the plots of the single modes because, due to the optimal resonator chosen, just the first one presented resonances (similarly to Fig.7).

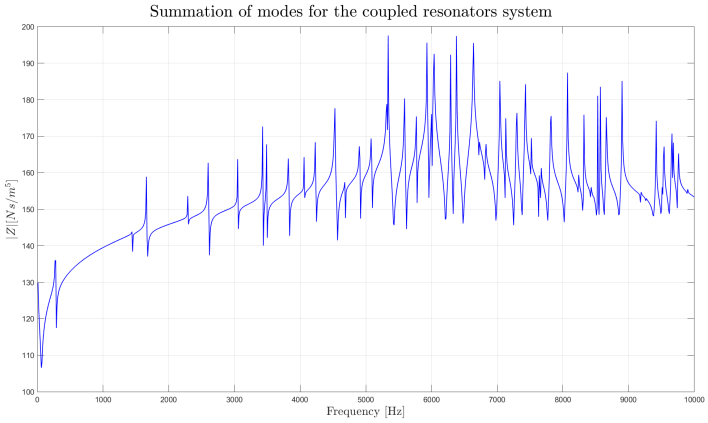

Figure 15: Impedance of the system considering the first four modes

The most evident consequence of the introduction of a second resonator is the presence of an additional resonance in the lower part of the spectrum. This pattern is also evident in the first harmonics, but it becomes more chaotic towards higher frequencies, where the different pairs start to overlap. We can also exploit COMSOL to visualize the nodal lines that characterize the modes of our system. In particular, thanks to the support of the GIF provided with this report, we can appreciate how these lines slowly travel through the object. The resonance condition happens when there is a zero of the pressure in correspondence of the entrance of the neck, and we can notice how for the first harmonics the pattern resembles that of the modes in a pipe. Increasing the frequency we can see how the nodal lines start to merge, also due to the resonance associated to the spherical part of the system. The exported file has been generated from the same results set of Fig.15 in the range [10, 2540] Hz but, differently from Fig.6, with a logarithmic scale for the amplitude and deselecting the option *synchronize scales between frames*.

f) Electric analog

An alternative way of studying acoustic systems is exploiting their electric analog that, when combined with a simulation software, can help us in validating our results. Before diving into the implementation of the circuit, we should point out the pros and cons of this kind of approach: in terms of computation costs and time they are both drastically reduced, but with the trade-off that the use of lumped elements imposes on the final accuracy of the analysis.

The electric analog of an Helmholtz resonator can be derived by carefully looking at the acoustic elements that compose it: the neck can be seen as a short pipe that presents losses due to viscous friction, whereas the volume of air is equivalent to a cavity. The first element can be associated with a component of inductance $L_i = \frac{\rho L}{S}$ paired with a resistor $R_i = \frac{\rho c}{S}$. Despite this theoretical model, we had to impose an arbitrary (smaller) resistance to better appreciate the results of the simulation: indeed, with a value in the order of the $M\Omega$, the dampening introduced would be too high to identify resonances. Since the impedance of a resistor does not depend on frequency, this alteration will not compromise the output of the analysis as far as concerns the location of the eigenfrequencies. The cavity is instead modeled by putting in series with the other two components a capacitor characterized by $C_i = \frac{V}{\rho c^2}$, closing an RLC loop. In Tab.2 all the values of the elements of the circuit are listed.

Component	R_1	R_2	C_1	C_2	L_1	L_2
Value	$1e-7[\Omega]$	$1e-7[\Omega]$	$1.03e-8[F]$	$1.47e-8[F]$	$224.58[H]$	$54.80[H]$

Table 2: Electrical analog components and associated values

At this point we have the analog of a generic resonator, but we need to properly connect the two elements of our system. To do so, we have to understand how the physical quantities act, in particular pressure: the cavity of the first resonator shares the same pressure with the neck of the second one, which in the equivalent circuit means connecting in parallel the two elements, as shown in Fig.16. The whole simulation has been run with a sampling frequency $Fs = 20[kHz]$, accordingly with the Nyquist Theorem, with a stop time of 5 seconds.

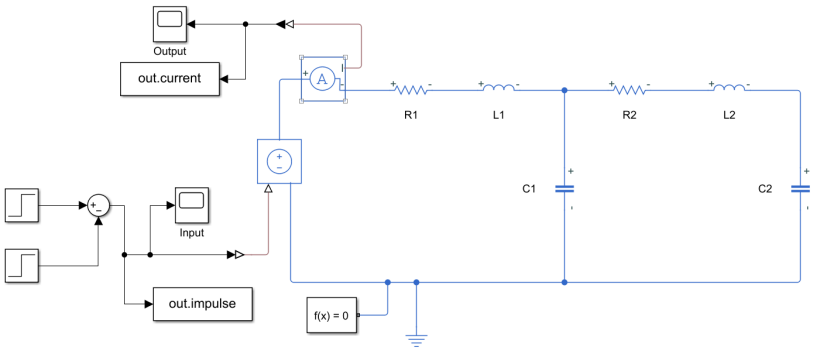

Figure 16: Simscape scheme for the electric analog of the coupled resonators

As concerns the excitation of the system, a combination of step functions has been used to feed a *controlled voltage source* with an impulse of one sample length, so that the whole frequency range of interest is included in the study. Right next to the generator we placed an amperometer to sense the current in the same point of the applied input. These two last quantities (electric analogs of the input pressure and the output acoustic volume flow) will be later sent to the Matlab workspace with the blocks *out.impulse* and *out.current*. The two time trends are finally processed through an FFT so that we can obtain the impedance Z as a function of frequency as the ratio input/output.

g) Compare and comment

In Fig.17 we plot the impedance of the system obtained in the previous section. The first noticeable difference is the choice of using a logarithmic frequency axis, which makes clearer the two resonances of the circuit. We have not opted earlier for this kind of representation because the model simulated in COMSOL had many additional resonances spread across the mid-high range of interest. The aforementioned difference of this kind of simulation is due to the meshing process: the system is subdivided in smaller portions and this allows the simulation to recognize all the resonances in the range of interest. The absence of these eigenfrequencies in the Simscape results comes instead from the limitation of using the lumped elements approximation. In particular, in this case we will be able to identify just a resonance for each LC pair and, due to the circuit's configuration, we will also observe a slight coupling between the two. Speaking of which, we should specify that the values of the inductances have been calculated considering a correction coefficient of 0.93 for the first neck, consistently with the first part of the study, and of 1.86 for the second one, due to its double-flanged configuration. Doing so we can appreciate the good level of approximation in terms of frequency matching between the two investigated approaches. Furthermore we noticed how changing L_1 would effect almost exclusively the position of the first resonance, and vice-versa for L_2.

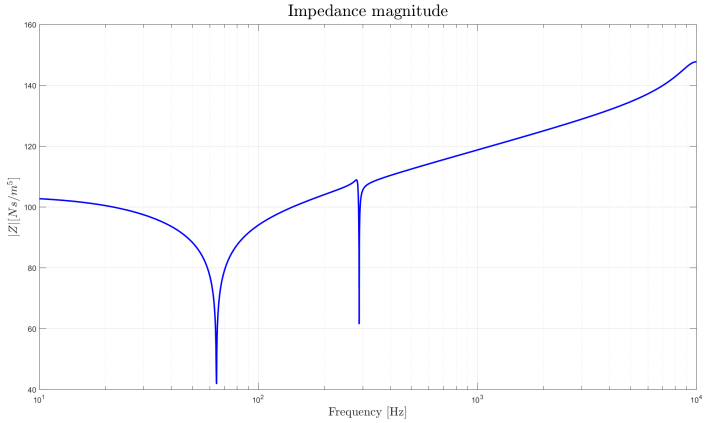

Figure 17: Impedance magnitude derived from the electric analog